



HAL
open science

Functionalization of magnetic chitosan microparticles – Comparison of trione and trithione grafting for enhanced silver sorption and application to metal recovery from waste X-ray photographic films

Mohammed Hamza, Adel A.-H. Abdel-Rahman, Mohamed Hawata, Rania El
Araby, Guibal Eric, Amr Fouda, Yuezhou Wei, Nora Hamad

► To cite this version:

Mohammed Hamza, Adel A.-H. Abdel-Rahman, Mohamed Hawata, Rania El Araby, Guibal Eric, et al.. Functionalization of magnetic chitosan microparticles – Comparison of trione and trithione grafting for enhanced silver sorption and application to metal recovery from waste X-ray photographic films. *Journal of Environmental Chemical Engineering*, 2022, 10 (3), pp.107939. 10.1016/j.jece.2022.107939 . hal-03684072

HAL Id: hal-03684072

<https://imt-mines-ales.hal.science/hal-03684072v1>

Submitted on 26 Jun 2024

HAL is a multi-disciplinary open access archive for the deposit and dissemination of scientific research documents, whether they are published or not. The documents may come from teaching and research institutions in France or abroad, or from public or private research centers.

L'archive ouverte pluridisciplinaire **HAL**, est destinée au dépôt et à la diffusion de documents scientifiques de niveau recherche, publiés ou non, émanant des établissements d'enseignement et de recherche français ou étrangers, des laboratoires publics ou privés.

Functionalization of magnetic chitosan microparticles – Comparison of trione and trithione grafting for enhanced silver sorption and application to metal recovery from waste X-ray photographic films

Mohammed F. Hamza^{a,b}, Adel A.-H. Abdel-Rahman^c, Mohamed A. Hawata^c, Rania El Araby^c, Eric Guibal^{d,*}, Amr Fouda^e, Yuezhou Wei^{a,f,**}, Nora A. Hamad^c

^a School of Nuclear Science and Technology, University of South China, Heng Yang 421001, China

^b Nuclear Materials Authority, POB 530, El-Maadi, Cairo, Egypt

^c Chemistry Department, Faculty of Science, Menofia University, Shebin El-Kom 32511, Egypt

^d Polymers Composites and Hybrids (PCH), IMT Mines Ales, Alès, France

^e Botany and Microbiology Department, Faculty of Science, Al-Azhar University, Nasr City, Cairo 11884, Egypt

^f School of Nuclear Science and Engineering, Shanghai Jiao Tong University, Shanghai, China

A B S T R A C T

Magnetic chitosan microparticles (MC) are successfully functionalized by grafting two pyrimidine derivatives (bearing either trione or trithione groups for MC-PYO and MC-PYS, respectively). The sorbents are characterized using SEM, TEM, BET, TGA, FTIR, titration, and elemental analysis. The study focuses on the comparison of the differential effects of functionalized groups on the sorption of silver. FTIR analysis shows the contributions of N-based, carbonyl, hydroxyl for silver binding onto MC-PYO, completed by sulfur contribution in the case of MC-PYS. Maximum sorption capacities at pH 6 reach 1.9 and 2.3 mmol Ag g⁻¹ for MC-PYO and MC-PYS, respectively. The Langmuir and the Sips equations fit sorption isotherms. The reactive groups affect the thermodynamic characteristics: endothermic for MC-PYS against exothermic for MC-PYO. The affinity of S-based soft ligand in MC-PYS for soft metals makes the sorbent selective for Ag(I). On the opposite hand, for MC-PYO the O-based functional groups readily bind hard metals (HSAB principle), meaning less selective for silver recovery (from multi-component solutions). QSAR method (quantitative structure-activity relationships) allows correlating preferentially sorption properties with the covalent index. Nitric acid solutions (0.3 M) are highly efficient for total desorption of silver from metal-loaded sorbents, but soft enough to maintain remarkable sorption and desorption performances for at least five cycles. The sorbents are successfully applied to Ag(I) recovery from acidic leachate of waste photographic films: metal removal is enhanced at pH 5.2; MC-PYS is more efficient and selective than MC-PYO at pH 2.2.

Keywords:

Sulfur-functionalization of magnetic chitosan microparticles
Silver sorption isotherms and uptake kinetics
Silver desorption and sorbent recycling
Sulfur-derivative for enhanced selectivity against competitor metals
Silver valorization from spent photographic film

1. Introduction

Silver is abundantly used in the jewelry industry as alloys with copper or with precious metals. These alloys may be also employed in computer and high-tech industries as electrical connectors. Based on its unique properties for visible light reflection, silver is also frequently involved in the confection of mirrors. The sensitivity of silver to light (and x-ray) makes it useful for high-quality photography and radiographic films [1], and for manufacturing photochromic lenses. Silver is also employed in button cell batteries [2], photovoltaics cells [3,4].

Silver resources are mainly reported in countries such as Peru, Mexico, China, Poland and Chile [5]. Most of the production comes as a sub-product from refining copper, cadmium, and zinc [6]. Various rates of silver recycling can be found in literature between 30 % and up to 80 % [6]. The wide dispersion of sources, the recovery of the metal as a by-product from the extraction of lead-zinc, copper, gold, or copper-nickel deposits, and the increasing recycling make the supply risk not critical (6.2/10 according RSC, [5]). The ingestion of silver may cause some health risks such as argyria (a pigmentation of skin and mucous membranes). The antimicrobial effect of silver may also cause

* Corresponding author.

** Corresponding author at: School of Nuclear Science and Technology, University of South China, Heng Yang 421001, China.
E-mail addresses: eric.guibal@mines-ales.fr (E. Guibal), yzwei@usc.edu.cn (Y. Wei).

some impact on the development of low microorganisms. These reasons may explain the development of processes for recycling silver from spent materials and decreasing its impact on the environment.

The silver (and co-metals) leachates from waste materials and effluents from industrial processes produce solutions that can be treated by precipitation and cementation (playing for example with the poor solubility of AgCl) [3,4,7,8]. Electrodeposition methods are also promoted for concentrated solutions [3,7,8]. Solvent extraction processes have been widely investigated for the recovery of silver from high concentration effluents [9–11]. In the case of less concentrated solutions, the sorption processes are generally more appropriate using chelating resin [12], biosorbents [13–15], or ion-exchange resin [16–19]. Sulfur-based sorbents have been designed making profit of the strong affinity of sulfur moieties for silver binding [12,16,20–22]. Though thiourea (and dithiooxamide, [12]) remains one of the most common sulfur-containing reagent grafted on polymer surfaces for improving silver sorption [23–28], alternative methods were also developed including immobilization of thiol derivatives [29,30], dithiocarbamate [31] or mercaptobenzimidazole [22].

Herein, chitosan was used as a support for manufacturing functionalized material. This aminopolysaccharide (commercially produced from shrimp shells) is hydrophilic (due to the presence of numerous hydroxyl and amine groups). These amine groups may bind metal anions in acidic solutions through ion-exchange/electrostatic attraction mechanisms (onto protonated amine groups). On the other hand, close to neutral pH, free amine groups may bind metal cations through chelation (onto the free electron doublet of nitrogen). However, this conjunction of hydroxyl and amine groups also helps in designing hydrogels under different shaping. Despite the hydrophilic behavior of chitosan, the compactness of the polymer network leads to substantial resistance to intraparticle diffusion; making sorption kinetics a critical criterion. Several strategies have been designed for overcoming this problem:

(a) synthesizing hydrogels (with network expansion, loss in crystallinity, and applying appropriate control of drying step),

(b) depositing the material at the surface of a porous support, or.

(c) decreasing the size of particles (with incorporation of magnetic particles to make easier the solid/liquid separation at the end of sorption process). This is precisely the strategy used in the current work for synthesizing functionalized magnetic chitosan microparticles (MC).

Being a soft Lewis acid (according Hard & Soft Acid & Base, HSAB, theory, [32]) silver will be more reactive with soft ligands (both in terms of kinetics and thermodynamic criteria). The objective of this research is designing new sorbents for enhancing the recovery of silver from aqueous solutions, with good selectivity against other competitor metal ions. Herein, two derivatives of MC microparticles are designed bearing pyrimidine derivatives, where the donor atoms have been varied; i.e., O (hard base, here MC-PYO) and S (soft base, here MC-PYS) donors. Another objective of this work consisted of evaluating the effect of different functional groups (based on pyrimidine unit) on both the sorption efficiency and metal selectivity (in agreement with HSAB) principles. The materials are characterized with SEM-EDX, FTIR, BET, TGA-DTA, elemental analysis, and titration facilities. The sorption properties of MC-PYO and MC-PYS for Ag(I) are compared with those of reference material (i.e., MC). The effect of pH on sorption capacity is investigated before carrying out uptake kinetics, sorption isotherms (and thermodynamics), the effect of metal cation competition (selectivity tests), metal desorption and sorbent recycling. The competition effect is analyzed in relation with the physicochemical specificities of the metals and the characteristics of grafted reactive groups (PYS vs. PYO). In the last part, the sorption process is tested for the treatment of leachates of wastes of X-ray photographic films.

2. Materials and methods

2.1. Materials

Lawesson reagent (97 %), glutaraldehyde solution (25 %, w/w), AgNO₃ (> 99 %), CdSO₄·xH₂O (≥ 99.99 %), chitosan (acetylation degree, DA: 25 %), epichlorohydrin (EPI, 98 %), anhydrous CaCl₂ (>97 %), diethyl malonate (99 %), urea (> 99 %), and sodium ethoxide (95 %), dimethyl formamide (DMF; 99.8 %), benzene (99.8 %) were provided by Sigma Aldrich (Merck KGa, Darmstadt, Germany). Sodium chloride, AlCl₃·6 H₂O (79.6 %), MgCl₂·6H₂O (91 %), ZnCl₂ (98.8 %), CuSO₄ (≥99.7 %) were obtained from Guangdong Guanghua, Sci-Tech Co., Ltd (Guangdong, China).

2.2. Synthesis and characterization of sorbents

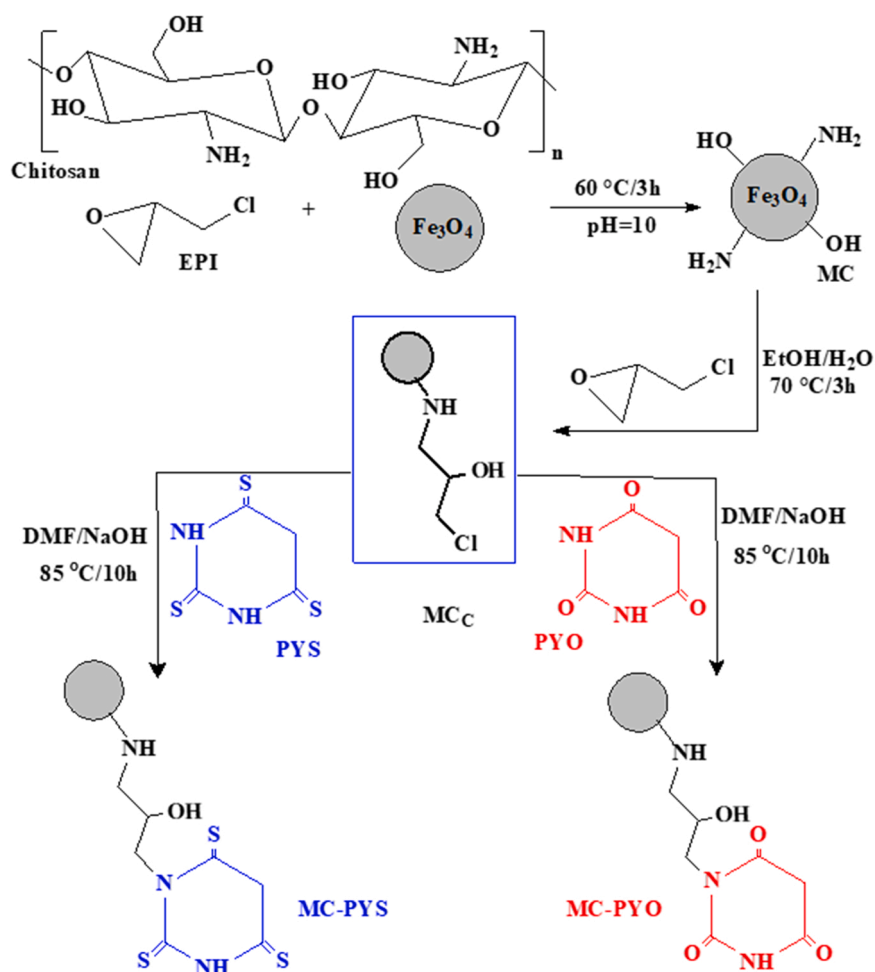
The synthesis of sorbents is detailed in Section A (see [Supplementary Information](#)). The Sections A.1 and A.2 report the synthesis routes for production of PYO and PYS precursors ([Schemes S1-S3](#)). First, the strategy consists of synthesizing magnetic chitosan microparticles by encapsulation of pre-formed magnetite nanoparticles (procedure derived from Massart [33], Section A3) with chitosan (mixing with biopolymer solution followed by alkaline precipitation). In a second step, the composite microparticles were successively crosslinked (MC) and activated (MCc) with epichlorohydrin (under different experimental conditions) to increase the stability of the material and to insert spacer arms (MC microparticles, considered as the reference material) ([Schemes S4-S5](#)). The functionalization of MC particles to produce MC-PYO and MC-PYS sorbents consisted in the grafting of PYO (barbituric acid) and PYS (PYO converted into sulfur-bearing derivative using the Lawesson Reagent) precursors onto the activated magnetic composite ([Section A.4, Scheme S6](#)). [Scheme 1](#) shows the expected structure of MC-PYO and MC-PYS sorbents.

The sorbents have been extensively characterized using SEM, and SEM-EDX facilities, BET measurements, TGA analysis, FTIR spectroscopy, titration, and elemental analysis. Detailed equipment and procedures are described in Section B, in SI.

2.3. Sorption tests

Sorption tests were performed using the batch method under mixing (v: 210 rpm). Metal-containing solutions (C₀, mmol Ag L⁻¹; V, volume, L, and initial pH₀) were mixed with known amounts of sorbent (m, g; sorbent dose, SD: m/V, g L⁻¹). Collected samples (fixed times for kinetics, or equilibrium) were filtrated using 1.2 μm-pore filter membrane (after magnetic separation), before being analyzed for metal content (C_{eq} or C(t), mmol Ag L⁻¹) by inductively coupled plasma atomic emission spectrometer (ICPS-7510, Shimadzu, Tokyo, Japan). The pH was not controlled during the sorption, but the equilibrium pH was systematically monitored (especially for detecting any unexpected variation and interference of alternative processes such as precipitation). Unless specified, standard temperature was T: 20 ± 1 °C (varied between 20 and 50 °C for the study of thermodynamics). For sorption isotherms, the initial metal concentration was set between 0.1 and 4.7 mmol Ag L⁻¹. The effective experimental conditions are systematically reported in the caption of the figures (see below). Similar experimental procedure was used for the investigation of sorption selectivity using equimolar multi-component solutions. For metal desorption from Ag-loaded sorbents, 0.3 M HNO₃ solution was used (and rinsing steps were processed using demineralized water between each run, when investigating sorbent recycling). The sorption capacity (concentration of metal ions in the sorbent, q, mmol g⁻¹) is obtained by the mass balance equation: $q = (C_0 - C_{eq}) \times V / m$. Experiments are obtained and represented in triplicate to show the reproducibility of sorption performances (preferentially to plotting less accurate averaged data).

The methods used for modeling uptake kinetics and sorption



Scheme 1. Synthesis of MC-PYO and MC-PYS and relevant structures.

isotherms are detailed in Section C (see SI).

2.4. Application to real effluents

The sorption process (using both MC-PYO and MC-PYS) was tested on a complex solution generated during the acid leaching of waste X-ray photographic film (see Section D in SI, for detailed procedures). The sorption process was carried out in batch, at room temperature (i.e., 21 ± 1 °C), under continuous agitation (210 rpm) by contact of the sorbent with the solution ($SD: 0.5 \text{ g L}^{-1}$) for 5 h. After magnetic separation, the concentration of metal ions was monitored by ICP-AES for calculating sorption capacities, selectivity coefficients, and distribution ratios.

Table 1
Summary of physicochemical properties of sorbents.

Parameter	Unit	MC	MC-PYO	MC-PYS	Technique	Figures	Tables
Particle size	μm		4–20 / Average: ~ 8.5		SEM	S1	
Magnetite NPs size	nm		Average: ~ 5		TEM	S2	
S_{BET}	$\text{m}^2 \text{g}^{-1}$		~ 65		N_2 / BET	S3	
Porous volume	$\text{cm}^3 \text{g}^{-1}$		0.55	0.705			
Pore size	\AA		566–487	459–420			
M_s	emu g^{-1}		12.3	19.2	VSM	S4	
Total weight loss	%		52.0	62.5	TGA	S5	
Magnetite content	%		48.0	37.5			
C content	mmol g^{-1}	26.79	28.20	23.48	EA		S4
N content	mmol g^{-1}	2.99	4.29	4.47			
O content	mmol g^{-1}	23.87	24.91	25.74			
S content	mmol g^{-1}			1.22			
pH_{PZC}		5.93	4.93	5.32	Titration	S9	

3. Results and discussion

3.1. Characterization of sorbents

Table 1 summarizes the main physicochemical characteristics of sorbent particles. The detailed discussion can be consulted in Section B (SI). SEM and TEM observations showed that the sorbents have comparable particle size (in the range 4–20 μm , average: 8.5 μm) with irregular tablet shapes (Fig. S1) with magnetite nanoparticles (~ 5 nm in size) (Fig. S2). The specific surface area (SSA) of sorbent particles is close to $65 \text{ m}^2 \text{g}^{-1}$; the pore distribution is affected by the type of substituent: MC-PYS being more porous than MC-PYO, in terms of pore volume but

with lower pore size (Fig. S3). The magnetite content also slightly differs with the sorbent (in the range 37.5–48 %) (Fig. S4), leading to different levels of saturation magnetization (MC-PYS > MC-PYO) (Fig. S4).

The chemical characterization is confirmed by FTIR analysis. Fig. S6 and Table S1 report the analysis of precursors (i.e., urea, PYO and PYS). Figs. S7 and S8 (completed by Tables S2–S3, for band assignments) show the FTIR analysis of the sorbents before and after Ag(I) sorption, and after 5 cycles of sorption and desorption. The magnetite nanoparticles are identified by strong bands at 590 or 542 cm^{-1} . The fingerprint of carbohydrate ring (chitosan) is detectable in the range 950–1150 cm^{-1} , while many other signals associated with C-N and N-H contributions (3450–3300 cm^{-1} overlapping of O-H and N-H stretching; N-H/NH-C=O bending at ~ 1620 – 1630 cm^{-1} ; and amine groups at 1350–1250 cm^{-1}). Multiple bonded C-O band is detected at 2180 cm^{-1} . Strong carbonyl bands (coming from chitosan and PYO “compartments”) are also detected for example at ~ 1680 cm^{-1} and ~ 790 cm^{-1} . In the case of MC-PYS, the presence of a band at 2511 cm^{-1} is usually assigned to S-H stretching (in thiol groups); meaning that tautomerization may affect the chemical structure of the functionalized sorbents (Scheme S7). The band at 637 cm^{-1} can be also assigned to C-S stretching vibration. The complexity of the sorbent where specific bands of chitosan can superpose to thione or trithione moieties make the assignment of the band relatively complex.

Elemental analysis shows the increase in the N-based content with functionalization (from 2.99 to 4.29–4.47 mmol N g^{-1}), while S-content reaches 1.22 mmol S g^{-1} in MC-PYS (Table S4). SEM-EDX analysis was used for the semi-quantitative characterization of the surfaces of materials (at different stages of the synthesis, and after metal sorption) (Tables S5 and b, Figs. S9 a and b). The presence of chlorine on activated MC (i.e., in MC_c) confirms the activation of the sorbent (reference material); while Cl element completely disappears after chemical grafting of PYO or PYS. The absence of chloride limits the possibility to precipitate silver as AgCl. The presence of S element confirms the efficient grafting of PYS. The successful chemical modifications of MC micro-particles are also confirmed by the variation of the pH_{PZC} values: from 5.93 for MC, it changes to 5.32 for MC-PYS, while MC-PYO is little more acid (i.e., 4.93) (Fig. S10).

3.2. Silver sorption

3.2.1. Effect of pH

Metal binding may be controlled by the pH through different effects: (a) metal speciation and (b) protonation/deprotonation of reactive groups. In the case of silver, the speciation is poorly affected by the pH in a wide range (Fig. S11, speciation diagram established using Visual Minteq, [34]): below pH 2, AgNO_3 may coexist (though as a minority, less than 17 %) with free Ag^+ ; and $\text{Ag}(\text{OH})$ precipitation may begin at $\text{pH} > 9.3$. Herein, the most significant effect of pH will concern the surface charge of the sorbents. Fig. 1 shows the comparison of pH-edges for Ag(I) sorption using MC, MC-PYO, and MC-PYS. The triplicate experiments clearly demonstrate the good reproducibility of sorption tests. Regardless of the type of sorbent, the sorption increases with pH from 1 up to 5–7, before stabilizing (above $\text{pH}_{\text{eq}} 5.3$ for MC, 6.8 for MC-PYS, and 6.3 for MC-PYO). In acidic solutions, the strong protonation of reactive groups (positive charge of the surface) causes strong electrostatic repulsion of Ag(I), correlated with a strong competition of protons with Ag^+ for binding onto reactive groups. With the pH increase, this repulsion decreases making more favorable cation binding onto free amine groups (onto chitosan units), and on either amine, carbonyl, or carbonothioyl groups. In the case of MC-PYO, sorption continuously increases with pH, while for MC-PYS the sorption capacity increases between pH 1 and 4.8 (or 5.9) before tending to stabilize: some of the reactive groups on MC-PYS become less reactive above pH 5.

Fig. 1 also provides preliminary information on the thermodynamics of Ag(I) sorption using MC-PYO and MC-PYS, which show reverse trends. Indeed, while increasing the temperature to 50 °C, the sorption

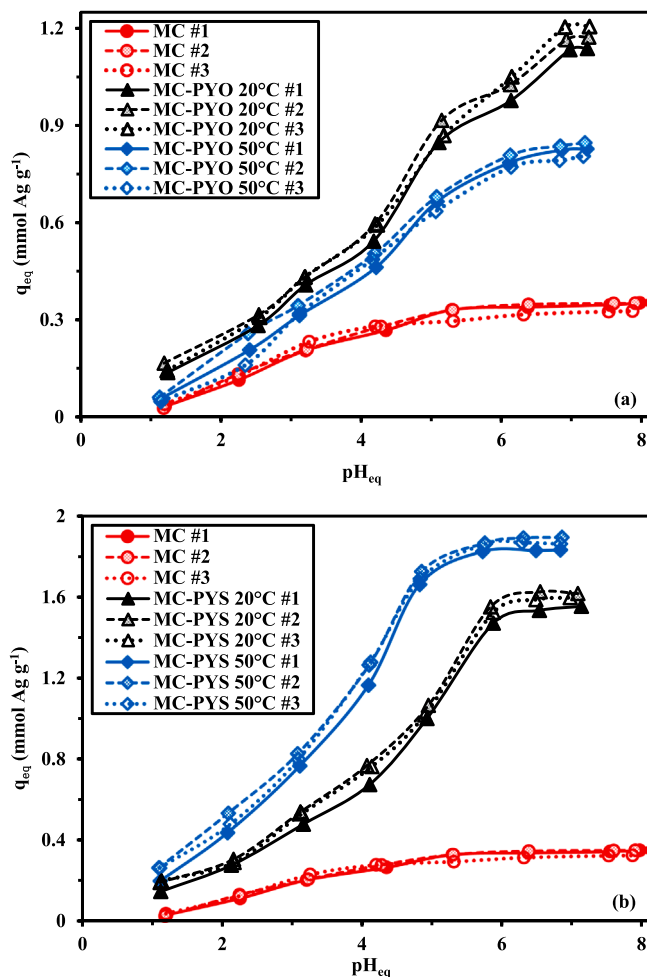


Fig. 1. Effect of pH_{eq} on the sorption of Ag(I) using MC, MC-PYO (a), and MC-PYS (b) sorbents (C_0 : 0.96 mmol Ag L^{-1} ; Sorbent dose, SD: 0.67 g L^{-1} ; v : 210 rpm; time: 48 h; T: 20 \pm 1 °C or 50 \pm 1 °C; triplicate series).

capacity tends to decrease (exothermic sorption), especially at pH higher than 4.2 for MC-PYO. A reciprocal trend is observed in the case of MC-PYS: sorption capacity globally increases with temperature (endothermic sorption) and the pH-edge curves are shifted toward lower pH values. MC-PYS sorption capacities are significantly higher than those of MC-PYO, especially when the pH is higher than 5. Under selected experimental conditions, at T: 20 °C and pH_{eq} : 6.8–7, the sorption capacity reaches $\approx 1.16 \pm 0.04$ mmol Ag g^{-1} for MC-PYO and up to $\approx 1.58 \pm 0.04$ mmol Ag g^{-1} for MC-PYS (only 0.32 mmol Ag g^{-1} for MC). Increasing the temperature expands the differences between MC-PYO and MC-PYS sorbents: $\approx 0.83 \pm 0.03$ mmol Ag g^{-1} and $\approx 1.87 \pm 0.03$ mmol Ag g^{-1} , respectively. The preference of silver (as soft acid) for ligands bearing soft atoms such as S-based ligands [32] may explain the higher sorption capacities obtained with MC-PYS. In addition, the reactivity of S-groups is apparently favored by high pH values (enhanced endothermic behavior). In addition, silver is known to readily precipitate in the presence of sulfide [35].

Fig. S12 shows pH variation during metal sorption. In the case of MC sorbent, the equilibrium pH slightly increases (proton binding by chitosan fraction). In the case of functionalized sorbents, the pH variations are relatively limited, especially for MC-PYO ($\Delta\text{pH} < 0.3$ pH unit); the highest variation is observed at pH 8 ($\Delta\text{pH} \approx 0.8$ pH unit). MC-PYS is more sensitive to pH: at pH higher than 6, the pH tends to decrease by 0.7–1 pH unit (proton release due to ion-exchange with Ag^+).

The distribution ratio D ($D = q_{\text{eq}}/C_{\text{eq}}$, L g^{-1}) can be plotted (in \log_{10} unit) against pH_{eq} (Fig. S13). In ion-exchange mechanisms, the slope of

the plot can be correlated to the stoichiometric ratio of proton exchange with metal cation. This can be extended to the stoichiometric ratio for proton release. Herein, it is not possible linearly correlating the distribution ratio with the pH. In the case of functionalized sorbents, MC-PYS shows good linear fit below $\text{pH}_{\text{eq}} 6$ at both T: 20 °C and 50 °C, while for MC-PYO, the linearity is only respected for T: 20 °C. The slopes are close to + 0.28 and + 0.33 for MC-PYS (at T: 20 °C and 50 °C, respectively), and + 0.23 for MC-PYO (at T: 20 °C).

3.2.2. Uptake kinetics

The uptake kinetics may be controlled by both resistance to diffusion (including bulk, film and intraparticle diffusion) and the proper reaction rate [36] in batch reactor. With a speed of agitation of 210 rpm, both particle settling and concentration gradients in the bulk of the reactor are minimized. In addition, previous studies have shown that this agitation speed allows neglecting the resistance to film diffusion (which is the predominant controlling step within the first minutes of contact). Therefore, the discussion of kinetic profiles (Fig. 2) is centered on the contributions of reaction rates (PFORE and PSORE, pseudo-first and pseudo-second order rate equations, respectively) and resistance to intraparticle diffusion (RIDE, or so-called Crank equation); the relevant equations are reported in Table S6a. The size of magnetic sorbent particles (about 8.5 μm) may explain that the uptake kinetics are fast: the equilibrium is reached within 60–90 min, and even faster in the case of MC-PYS (where 30–60 min of contact are sufficient). The superposition of the kinetic profiles for duplicated series demonstrates the reproducibility of experimental data. The residual relative concentrations follow the expected trend $\text{MC} \gg \text{MC-PYO} > \text{MC-PYS}$, consistently with the comparative sorption capacities revealed in the previous section. The initial slope of kinetic profiles also follows the same order. This higher affinity of silver for the reactive groups of MC-PYS (compared with those of MC-PYO) influences both the equilibrium and the mass transfer behavior. In addition, silver transfer may be affected by the textural properties of the sorbents. Actually, the two sorbents have the same order of magnitude for S_{BET} , with higher porous volume and smaller pore size for MC-PYS. Despite its lower pore size, the mesoporous structure of MC-PYS is not hindering the diffusion of silver ions. Table 2 summarizes the parameters of the three models. The comparison of both calculated and experimental values for equilibrium sorption capacities and statistical parameters (i.e., R^2 and AIC values) clearly demonstrate the superiority of the PFORE for fitting kinetic profiles over PSORE and RIDE. In Fig. 2, the lines superposed to experimental points show the fitting of kinetic profiles with the PFORE. The model fails to fit the time range at higher curvature (around 25–40 min); however, the fits are much better than those obtained with the PSORE and RIDE (Fig. S13).

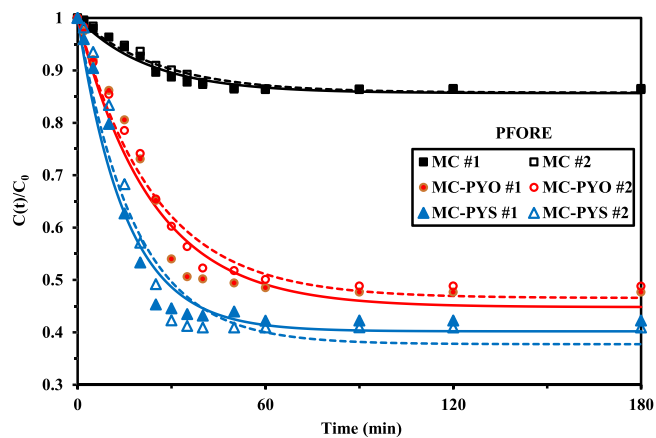


Fig. 2. Ag(I) uptake kinetics using MC, MC-PYO, and MC-PYS at T: 20 \pm 1 °C – Modeling with PFORE (pH_0 : 6; C_0 : 0.96 mmol Ag L^{-1} ; Sorbent dose, SD: 0.4 g L^{-1} ; v : 210 rpm; duplicate series).

Several recent contributions have shown how is risky the discussion and interpretation of PFORE and PSORE fits when experimental conditions are not fulfilling the model requisites [37,38]. Indeed, concluding that model fits can be correlated to systems controlled by either physi- or chemisorption is only possible when a series of conditions are satisfied. One of the most frequently neglected concerns the variability of the concentration in the solution. Correct application of the models requires getting a system where the concentration negligibly varies in the reactor. This is not the case in the current work, except (to a certain extent) for MC sorbent (where the concentration varies by less than 14 %). Therefore, the equations are only used for comparing the apparent rate coefficients for the three sorbents. Table 2 shows that MC and MC-PYO have comparable k_2 values ($4.34\text{--}3.87 \times 10^{-2} \text{ min}^{-1}$ and $4.24\text{--}4.11 \times 10^{-2} \text{ min}^{-1}$, respectively); little lower than for MC-PYS (i. e., $6.52\text{--}5.51 \times 10^{-2} \text{ min}^{-1}$).

It is noteworthy that though the sorption is globally rapid, faster kinetics would be expected taking into account the small size of the sorbents (i.e., 8.5 μm). This means that the contribution of the resistance to intraparticle diffusion cannot be formally neglected. Table 2 also reports the estimated values of the effective diffusivity coefficient (D_e); these values are remarkably stable for the three sorbents in the range $1.05\text{--}1.55 \times 10^{-13} \text{ m}^2 \text{ min}^{-1}$. This is several orders of magnitude lower than the self-diffusivity of silver in water (i.e., D_0 : $9.89 \times 10^{-8} \text{ m}^2 \text{ min}^{-1}$) [39]. This is another confirmation of the contribution of the resistance to intraparticle diffusion to the control of Ag(I) sorption kinetics. Despite the decrease in particle size, the intrinsic poor porosity of chitosan maintains diffusion constraints. Using freeze-drying at each step of the synthesis procedure could probably soften this effect, at least partially.

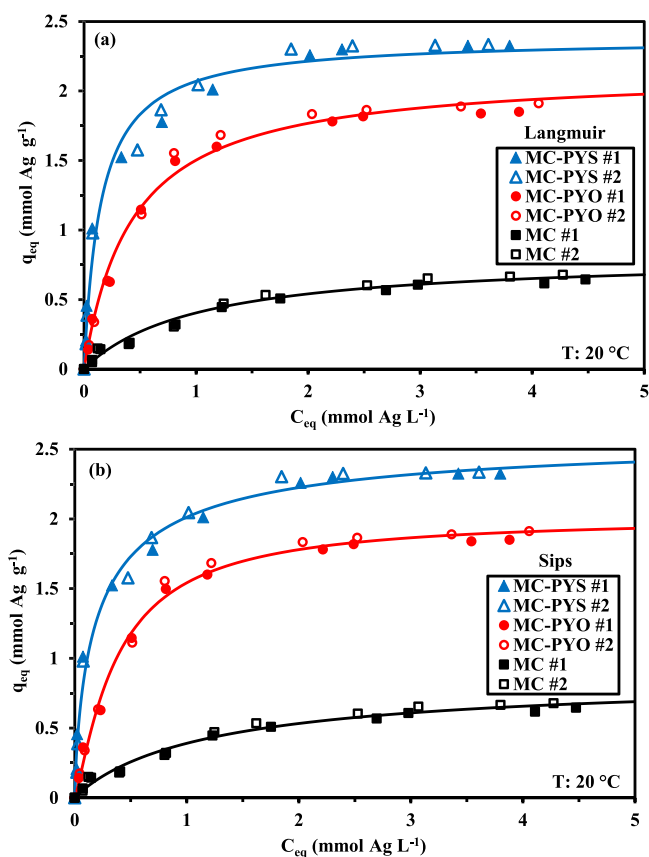
3.2.3. Sorption isotherms

The sorption isotherms ($q_{\text{eq}}=f(C_{\text{eq}})$) are compared for the three sorbents in Fig. 3, at $\text{pH}_0 6$ and at room temperature (20 ± 1 °C). The superiority of MC-PYS over MC-PYO is illustrated by the comparison of maximum sorption capacity (higher saturation plateau 2.33 vs. 1.91 mmol Ag g^{-1}) and affinity (steeper initial slope). This figure also shows the benefit of MC functionalization: maximum sorption capacity does not exceed 0.68 mmol Ag g^{-1} for reference material. MC binds silver through free amine and hydroxyl groups on the sorbent. For functionalized materials, the new reactive groups (pyrimidine moiety, amine, hydroxyl, carbonyl, or carbonothioyl groups) bring supplementary binding sites. Silver being a soft acid preferentially reacts with soft bases. Therefore, MC-PYS, which differs on the pyrimidine cycle from MC-PYO by substitution of -one by -thiol groups, is expected to have a stronger affinity for silver. This is consistent with the trends observed in Fig. 1. The power-type Freundlich equation is not appropriate for describing the sorption isotherms that are characterized by the appearance of saturation plateaus. Table 3 summarizes the parameters of the usual models (described in Table S6b); the calculations were performed cumulating the duplicate series (the calculation for individual series is reported in Table S7). The comparison of statistical criteria confirms that the sorption isotherms are preferentially fitted by the Langmuir and the Sips equations: the differences in fitting quality is associated with difference in AIC values greater than 2 (the lower the AIC, the better being the quality of the fit). The Sips equation fits globally better experimental profiles than the Langmuir equation. The Langmuir equation supposes the sorption to proceed as a monolayer, without interaction between sorbed molecules and with homogeneous distribution of sorption energies. The Sips equation is a combination of Langmuir and Freundlich equations; the third-adjustable parameter lightly improves the quality of the mathematical fit, at the expense of a loss in the physical significance of the fit. It is noteworthy that the Temkin equation does not fit well MC and MC-PYO isotherms, contrary to MC-PYS (good simulation). The Temkin sorption isotherm supposes that (a) the sorption heat of sorbate linearly decreases with the progressive saturation of the sorbent surface, and (b) the binding energies to

Table 2

Ag(I) uptake kinetics using MC, MC-PYO, and MC-PYS – Parameters for PFORE, PSORE, and RIDE models.

Sorbent			MC		MC-PYO		MC-PYS	
Model	Parameter	Run	#1	#2	#1	#2	#1	#2
PFORE	$q_{eq,exp}$		0.337	0.319	1.20	1.23	1.40	1.39
	$q_{eq,1}$		0.354	0.335	1.26	1.28	1.45	1.47
	$k_1 \times 10^2$		4.34	3.87	4.24	4.11	6.52	5.51
	R^2		0.976	0.979	0.964	0.984	0.971	0.964
	AIC		-140	-143	-93	-107	-93	-87
PSORE	$q_{eq,2}$		0.424	0.405	1.52	1.54	1.67	1.72
	$k_2 \times 10^2$		11.2	10.2	3.01	2.90	4.74	3.67
	R^2		0.944	0.952	0.930	0.958	0.930	0.919
	AIC		-130	-133	-85	-95	-83	-78
	$D_e \times 10^{13}$		1.16	1.49	1.10	1.05	1.55	1.31
RIDE	R^2		0.953	0.959	0.931	0.959	0.937	0.924
	AIC		-127	-129	-82	-90	-80	-74

Units: q , mmol L^{-1} ; k_1 , min^{-1} ; k_2 , $\text{g mmol}^{-1} \text{min}^{-1}$; D_e , $\text{m}^2 \text{min}^{-1}$.**Fig. 3.** Ag(I) sorption isotherms using MC, MC-PYO, and MC-PYS sorbents – Modeling with the Langmuir (a) or Sips (b) equation (at pH_0 6, C_0 : 0.093–4.64 mmol Ag L^{-1} ; T : 20 ± 1 °C, time: 48 h; v : 210 rpm).

be uniformly distributed (up to a maximum binding energy). The difference observed for MC-PYS (associated with sorption energies) is consistent with the reciprocal trends observed between MC-PYO and MC-PYS for the effect of temperature (study of pH effect, Section 3.2.1.). In Table 3, the comparison of the parameters for the Langmuir equation shows that the calculated and experimental sorption capacities at saturation of the monolayer are consistent (overestimation by less than 10 % for calculated value) for functionalized sorbents. The affinity coefficient (i.e., b_L) is significantly increased according: MC (0.87 L mmol^{-1}) < MC-PYO (2.33) < MC-PYS (6.68). In the case of the Sips equation, the affinity coefficients are of the same order of magnitude for MC-PYO and MC-PYS (3.24 – 3.32 L mmol^{-1}) but the exponential term (i.e., n_S) significantly increases for the sorbent bearing carbonothioyl moieties

Table 3Ag(I) sorption isotherms using MC, MC-PYO, and MC-PYS – Parameters for Langmuir, Freundlich, Sips, and Temkin models (at T : 20 ± 1 °C; calculations on combinations of Runs #1 and #2).

Sorbent		MC	MC-PYO	MC-PYS
Model	Parameter			
Experimental	$q_{m,exp}$	0.678	1.91	2.33
	$q_{m,L}$	0.844	2.15	2.38
Langmuir	b_L	0.870	2.33	6.68
	R^2	0.982	0.991	0.982
	AIC	-141	-110	-88
	k_F	0.364	1.31	1.79
	n_F	2.22	2.91	3.66
Freundlich	R^2	0.961	0.921	0.941
	AIC	-125	-64	-62
	$q_{m,S}$	0.875	2.02	2.62
	b_S	0.809	3.24	3.32
	n_S	1.05	0.828	1.30
Sips	R^2	0.982	0.994	0.989
	AIC	-139	-115	-94
	$A_T \times 10^{-3}$	15.06	31.44	117.9
	b_T	15,695	5868	6,026
	R^2	0.957	0.975	0.989
Temkin	AIC	-115	-89	-98

Units: q , mmol g^{-1} ; b_L , L mmol^{-1} ; n_F and n_S , dimensionless; k_F , $\text{mmol}^{(1-1/n_F)} \text{g}^{-1} \text{L}^{1/n_F}$; A_T , L mol^{-1} ; b_S : $(\text{mmol L}^{-1})^{n_S}$; b_T , kg mol^{-2} .

from 0.828 to 1.30.

The study of pH effect has previously shown the opposite trends of MC-PYO and MC-PYS in terms of temperature effect. This unexpected behavior motivates a more complete study of thermodynamic criteria. The sorption isotherms have been carried out at T : 20, 30, 40, and 50 °C (Fig. 4). The evolutions are consistent with previous conclusions:

(a) Ag(I) sorption strongly decreases with increasing temperature, for MC-PYO: the sorption of silver is exothermic (q_m decreases from 1.9 to $1.2 \text{ mmol Ag g}^{-1}$),

(b) Ag(I) sorption increases with temperature for MC-PYS: the sorption of silver is endothermic (q_m increases from 2.3 to $3.1 \text{ mmol Ag g}^{-1}$).

It is noteworthy that the initial slope (correlated with the affinity of the sorbent for silver) is also significantly affected by temperature in the case of MC-PYO, while the impact is moderate in the case of MC-PYS. This is confirmed by the progressive decrease of b_L in Table S8 for MC-PYO (calculations made for cumulated series; Table S9 shows the individual calculations for the duplicated series). The Sips equation (represented in Fig. 4) fits better experimental profiles but the specific affinity coefficient does not follow a clear trend, because of the simultaneous variation of the exponential term (n_S , which decreases with temperature). In the case of MC-PYS, the best fits are obtained with the Sips equation and even better with the Temkin equation (Tables S10 and

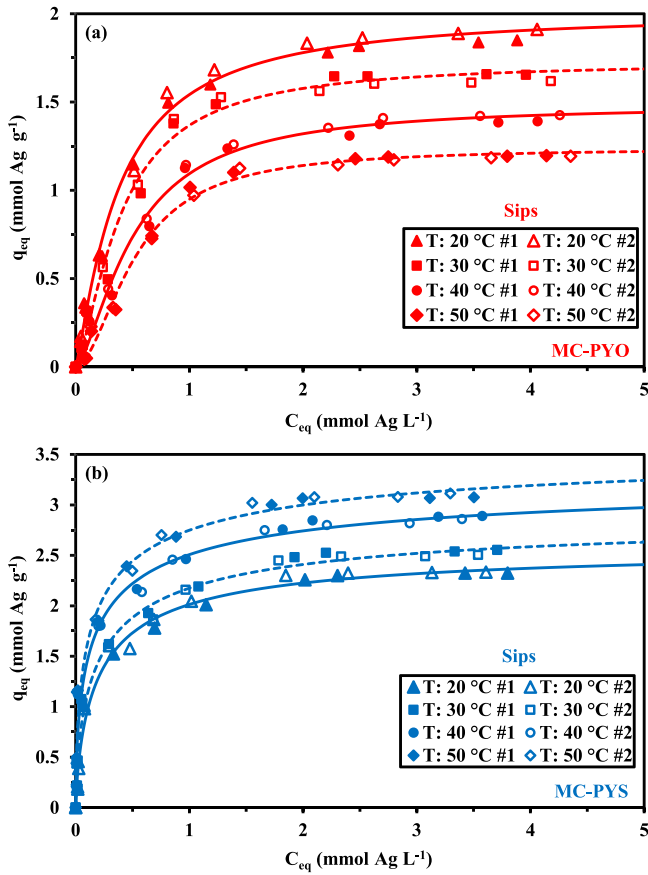


Fig. 4. Effect of temperature on Ag(I) sorption isotherms using MC-PYO (a), and MC-PYS (b) sorbents – Modeling with the Sips equation (at pH₀ 6, C₀: 0.093–4.64 mmol Ag L⁻¹; T: 20–50 ± 1 °C, time: 48 h; v: 210 rpm).

S11). Again, the variation of b_S does not show a clear trend, which is associated with the increase of the value of the exponential factor (i.e., n_S). The parameter b_T hardly varies with the temperature (in the range, b_T : 6026–6236 J kg mol⁻²), contrary to the parameter a_T that progressively increases with temperature from 117.9×10^3 to 421.3×10^3 L mol⁻¹.

These differences clearly illustrate that the mechanisms involved in silver sorption strongly differ between MC-PYO and MC-PYS. Physical sorption is frequently (though not exhaustively) exothermic. In the case of chemisorption, the required activation of the solute may explain that the sorption increases with temperature, at least in a certain range of temperature, while increasing more the temperature, the sorption may come back to the adverse effect of temperature; this was not observed between 20 and 50 °C.

The thermodynamic parameters may be calculated using the van't Hoff equation [40]:

$$\Delta G^\circ = \Delta H^\circ - T\Delta S^\circ \quad (1a)$$

where ΔG° and ΔH° are the changes in Gibbs free energy and enthalpy (in kJ mol⁻¹), and ΔS° is the entropy change (J mol⁻¹ K⁻¹). The change in Gibbs free energy can be associated with the standard thermodynamic equilibrium constant (K_{eq}° , based on molar concentrations) according to:

$$\Delta G^\circ = -RT \ln K_{eq}^\circ \quad (1b)$$

$$\ln K_{eq}^\circ = \frac{-\Delta H^\circ}{R} \frac{1}{T} + \frac{\Delta S^\circ}{R} \quad (1c)$$

The expression of K_{eq}° depends on the sorption isotherm and can be

associated to the parameters of the models (in molar units) according specific conversions reported by Tran et al. [40]. In the case of Langmuir equation, K_{eq}° is calculated using:

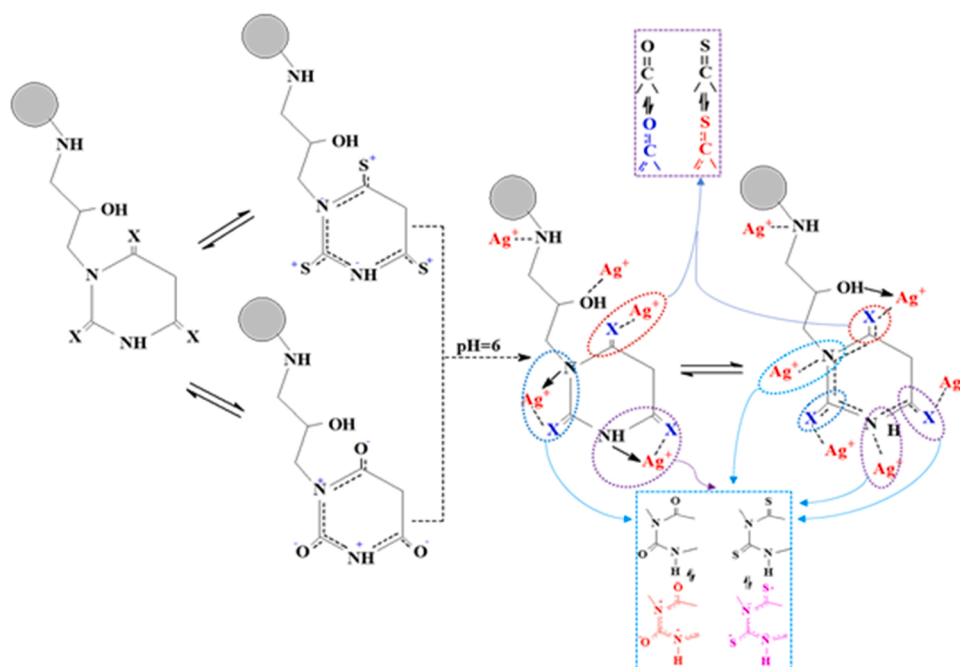
$$K_{eq}^\circ = b_L \frac{C_{sorbate}^\circ}{\gamma_{sorbate}} \quad (1d)$$

where $C_{sorbate}^\circ$ is the unitary standard concentration of the sorbate (i.e., ~ 1 mol L⁻¹) and $\gamma_{sorbate}$ is the activity coefficient of the sorbate (for dilute solutions, $\gamma \sim 1$). The van't Hoff equation was applied after relevant corrections of standard thermodynamic constants for the individual data (not joining duplicate isotherms) collected from Table S9 and Table S11. Fig. S15 shows the van't Hoff plots, while Table S12 reports the thermodynamic parameters. The negative values of the change in Gibbs energy confirms the spontaneity of the sorption process. For MC-PYO, the Gibbs free energy hardly changes with temperature, while for MC-PYS, the spontaneity is improved by the temperature. As expected from the effect of temperature on sorption isotherms, the enthalpy change is positive (+26.32 kJ mol⁻¹) for the endothermic sorption of Ag (I) onto MC-PYS, contrary to MC-PYO that shows a negative enthalpy change (-16.38 kJ mol⁻¹), which reflects the exothermic nature of silver binding. In the case of amino-carbamate grafted alginate, Shehzad et al. [41] reported that silver sorption is exothermic. For the two functionalized sorbents, the entropy change is positive, meaning that the randomness increases with metal sorption. The entropy change is weak for MC-PYO compared with MC-PYS (12.25 vs. 157.4 J mol⁻¹ K⁻¹). The sorption of silver is accompanied by deprotonation of reactive groups (ion-exchange), by chelation (ligand exchange at the side of Ag⁺: nitrate vs. reactive groups onto the sorbent) and by partial dehydration of silver aqua complex (i.e., Ag(H₂O)₄⁺). These different mechanisms may explain the increased randomness of the system after metal sorption; their contributions are different for the two sorbents leading to substantial differences in the entropy changes.

The sorption of silver using functionalized MC shows good sorption performances compared with alternative sorbents (Table S13). Actually, MC-PYS shows comparable sorption properties to the characteristics reported by Wu et al. [42] for activated carbon (recovered from supercapacitor devices). It is noteworthy that the sorption capacity is roughly halved when using recycled supercapacitor AC. Some materials have outstanding sorption capacities, such as dithioamide/formaldehyde resin ($q_{m,L}$: 30.9 mmol Ag g⁻¹) [12], or nanoscale zerovalent iron deposited onto activated carbon ($q_{m,L}$: 12.0) [43], dithiocarbamate functionalized cellulose ($q_{m,L}$: 9.94) [44], or thio-grafted magnetic polypyrrole ($q_{m,L}$: 7.48) [45]. In recent literature, other materials bearing S-based reactive groups show maximum sorption capacities comparable to those herein reported for MC-PYO and MC-PYS: thiourea-PVDF membrane ($q_{m,L}$: 1.86 mmol g⁻¹) [28], mercaptobenzimidazole chitosan ($q_{m,L}$: 2.02) [22]. Combining criteria such as sorption capacities, and kinetic characteristics, MC-PYS reveals one of the most efficient sorbents for Ag(I) sorption at pH close to 6.

3.2.4. Sorption mechanism

Actually, there is a symmetry between O and S groups substituted onto pyrimidine ring (for MC-PYO and MC-PYS, respectively). The tautomerization mechanism appended in left side shows the effect on the structure of reactive groups and their potential reactivity for Ag(I) cations: O⁻ reactive groups can bind Ag⁺ by ionic interaction, while S⁺ reactive groups may bind Ag⁺ by chelation in tautomerized forms. This could explain that the thermodynamic properties of the two sorbents are inversed (endo vs. exo-thermic). Scheme 2 shows tentative mechanisms for Ag(I) sorption onto MC-PYO and MC-PYS sorbents based on the effect of pH on metal sorption, sorption isotherms (molar ratio at saturation of the sorbents) and thermodynamic criteria (possible distinction between chemi- vs. physisorption). Compared with pristine MC sorbent, the grafting of PYO leads to an increase in maximum sorption capacity ($q_{m,L}$) close to 1.29 mmol Ag g⁻¹, while the reactive groups are increased by



Scheme 2. Tentative mechanisms involved in Ag(I) sorption onto sorbents.

1.30 mmol N g⁻¹ and 1.04 mmol O g⁻¹. In the case of MC-PYS sorption capacity increases by 1.54 mmol Ag g⁻¹ (vs. MC); N and O content increasing by 1.48 mmol N g⁻¹ and 1.87 mmol O g⁻¹, respectively; in addition to the appearance of 1.22 mmol S g⁻¹. There is a direct correlation between the increase in N-content and the increase in sorption properties; though other functional groups are involved in the binding mechanism (stabilization of metal binding according Ag(I) coordination number). Metal sorption increases with the pH and reaches its maximum close to the pH_{PZC} value for MC and MC-PYS, while for MC-PYO, the sorption capacity increases above its specific pH_{PZC} value.

Silver sorption induces significant changes in the FTIR spectra of MC-PYO (Fig. S7, Table S2) and MC-PYS (Fig. S8, Table S3). The broad band around 3385–3449 cm⁻¹ (which corresponds to the overlapping of N–H and O–H stretching vibrations) is systematically affected (in terms of both relative intensity and wavenumber shift). This means that silver binding involves amine groups (from chitosan backbone and/or from pyrimidine ring, as “normal” or tautomeric forms) and/or OH functional groups (including for filling the coordination sphere). For MC-PYO, the contribution of N-based groups is also confirmed by the shifts in the band at 1631 cm⁻¹ (broad band convoluting N–H bending and carbonyl stretching) to 1573 cm⁻¹ (apparently, the contribution of the carbonyl vibration strongly decreases), and the bands in the range 1500–1250 cm⁻¹ (C–O, C–N and N–H groups). A strong band appears at 553 cm⁻¹ (overlapping to the magnetite contribution at 590 cm⁻¹). For this sorbent, metal binding involves carbonyl, hydroxyl and N-based groups. It is noteworthy that metal desorption restores relatively well the sorbent (as confirmed by the FTIR spectrum obtained after the fifth desorption cycle). In the case of MC-PYS, the FTIR spectrum is drastically changed after silver binding. The band at 3449 cm⁻¹ is strongly decreased in relative intensity and the extremum is shifted toward 3084 cm⁻¹: amine and hydroxyl groups are implicated in silver bonding. The contribution of carbohydrate fingerprint is drastically reduced. However, the most significant changes are observed in the regions 1720–1600 cm⁻¹ and 1450–1200 cm⁻¹. The broad band (with band doublet at 1679 and 1627 cm⁻¹) is replaced with three bands (at 1714, 1637, and 1560 cm⁻¹); apparently, a carboxylic group unexpectedly appears at 1714 cm⁻¹. In this area, C=O and N–H bands are influenced (directly or in their neighborhood). On the other hand, the bands at 1412, 1360, 1303 cm⁻¹, which may be assigned to the contributions of

C–N (in pyrimidine ring), C–O stretching, and amine groups, are strongly reduced or at least significantly shifted. The 2511 cm⁻¹ peak (tautomeric thiol) disappears after metal sorption: the environment of S groups is affected by metal binding. After the fifth desorption step, the FTIR spectrum is globally restored. However, some shifts and changes in relative intensities are observed, showing that the sorbent is irreversibly affected by metal sorption. Surprisingly, the strong bands at 856, 790 and 768 cm⁻¹ totally disappear in the recycled sorbent.

3.2.5. Sorption selectivity

Real effluents are constituted of complex solutions containing a wide diversity of metal ions. The potential of new sorbents cannot be really estimated without considering the impact of multi-component solutions onto the sorption of target metals. Herein, the sorption of Ag(I) was tested using MC-PYO and MC-PYS in the treatment of multi-component equimolar solutions (containing 1 mmol L⁻¹ of Na(I), Ca(II), Mg(II), Cd(II), Zn(II), and Cu(II), in addition to Ag(I)). Sorption tests were processed at different pH values (between 4 and 8) to check the possibility of separating silver from competitor metals with appropriate selection of pH conditions. Fig. S16 shows the log₁₀ plot of distribution ratio ($D = q_{eq}/C_{eq}$, L g⁻¹) vs. pH_{eq}. Both MC-PYO and MC-PYS show marked preference for silver binding from multi-metal solutions, according:

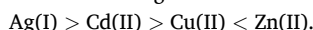
For MC-PYS: Ag(I) > Cd(II) > Cu(II) > Mg(II) > Na(I) ≈ Ca(II) ≈ Zn(II).

For MC-PYO: Ag(I) > Cd(II) > Cu(II) > Mg(II) > Na(I) ≈ Ca(II) ≈ Zn(II), below pH 6 and.

Ag(I) > Cu(II) > Cd(II) > Mg(II) > Na(I) ≈ Ca(II) ≈ Zn(II), above pH 6.

The distribution ratio also increases with the pH. However, in the case of Cu(II) the slope of the increase is significantly more marked than for other cations; this is probably associated with the formation of copper hydroxides and colloidal species (which may precipitate at the higher pH values), or the effect of sorbent deprotonation. The order of selectivity cannot be directly correlated with individual criteria (See Table S14, which summarizes the physicochemical properties of selected metal cations). The preference of the sorbents for Ag(I), Cd(II) and Cu(II) is consistent with their classification as soft or intermediary HSAB metals (and softness criterion); however, Zn(II), which is also ranked among intermediary acids, shows less coherent behavior.

Table S15 reports the distribution ratio for MC-PYO and MC-PYS and heavy metal ions, at two pH values around 6. These data confirm the preferential binding of metal ions according:



The capacity to separate Ag(I) from other metal cations is evaluated using the selectivity coefficient ($SC_{\text{Ag}/\text{Metal}}$):

$$SC_{M1/M2} = \frac{D_{M1}}{D_{M2}} = \frac{q_{eq,M1} \times C_{eq,M2}}{C_{eq,M1} \times q_{eq,M2}} \quad (2)$$

Fig. 5 compares the selectivity coefficients for Ag(I) against the different metals at different pH values, for both MC-PYO and MC-PYS. The $SC_{\text{Ag}/\text{Metal}}$ values are globally superior for MC-PYS compared with MC-PYO. However, some differences can be identified:

(a) The selectivity for Ag(I) against Cd(II) is lower in the case of MC-PYS (compared with MC-PYO). Cadmium(II) is part of soft acids as Ag(I); this favors the sorption of Cd(II) onto MC-PYS. This contributes to decrease the selective separation of the two metal cations,

(b) the impact of the pH (neutral pH) is apparently more marked for MC-PYS, while MC-PYO shows good performances also at $\text{pH}_{\text{eq}} 5.25$. This is consistent with the acid-base properties (pH_{pZC} values) of the sorbents, and the relative effect of pH on sorption performances (Section 3.2.1.).

Figs. S17 a and b show the distribution of bound metals onto MC-PYO and MC-PYS, at $\text{pH}_{\text{eq}} \approx 7.7$. In this figure, MC-PYS confirms its preference for Ag(I) over Cd(II) and Cu(II). This selectivity is higher than for MC-PYO. Fig. S17c reports the cumulative sorption capacities. The profiles are superposed for the two sorbents up to $\text{pH}_{\text{eq}} \approx 5.2$. At higher pH, the cumulative sorption capacity of MC-PYO overpasses that of MC-PYS (1.99 vs. 1.72 mmol g^{-1}). MC-PYS having a higher affinity for soft metals (which are underrepresented compared with hard metals); the total sorption capacity is logically higher for MC-PYO (which has higher binding affinity for hard acids). Sulfur-based ligands (soft) have higher

affinity for soft metal ions (such as Ag^+ or Cd^{2+}), while O-bearing ligands are more favorable for hard metal binding (such as Na^+ , Ca^{2+} , Mg^{2+}) [32].

QSAR (qualitative structure activity relationship) facilities [46] were used for correlating metal sorption properties in multi-component solutions with their specific physicochemical criteria (see QSAR approach in SI). The better correlation is found between sorption capacity and the covalent index ($X_m^2 \times r$), where X_m is the Pauling electronegativity and r the ionic radius of the metal ion (Fig. S18). This conclusion confirms that metal sorption is mainly driven by chelation mechanism (though mediated by acid-base properties and ion-exchange under the control of protonation of reactive groups).

3.2.6. Metal desorption and sorbent recycling

The potential of a new sorbent is also strongly controlled by the possibility to recycle the material. The strong sensitivity of silver sorption to pH gives a first orientation for choosing an acidic solution for reversing metal binding. The presence of magnetite, which may be partially dissolved by excessive acid conditions [47], requires using mild concentrations. Previous studies have shown that nitric acid solutions are less aggressive for magnetite than sulfuric acid. Logically, the dissolving of magnetite is controlled by temperature and acid concentration [47]. With processing at room temperature and at mild concentration of nitric acid, the loss of magnetite nanoparticles may be minimized, especially as embedded composite particles. Previous experiments on another type of magnetic-based chitosan sorbent has shown that after the contact of the sorbent with an acidic solution the loss of iron (from magnetite) does not exceed 1 % when HCl concentration remains below 0.5 M [48]. Silver desorption is investigated using 0.3 M HNO_3 solution; desorption kinetics are reported in Fig. S19. Under selected experimental conditions, 20–30 min of contact are sufficient for achieving the complete elution of silver.

After careful washing with demineralized water, the sorbent can be recycled. Table 4 reports the sorption and desorption efficiencies over 5 cycles. MC-PYO and MC-PYS show remarkable stability in performances: complete desorption at each cycle, and a progressive weak loss in sorption efficiency that remains below 2.5 % at the fifth cycle. Functionalized sorbents are more resilient than raw MC that shows a loss in sorption efficiency slightly higher than 10.6 % at the last cycle (though complete desorption of silver is maintained). It is noteworthy that the FTIR analysis on the sorbent after five cycles of sorption and desorption showed significant changes in the spectra (especially for MC-PYS). These changes confirm that the alternating cycles (involving different acid/neutral pH conditions) strongly affect the chemical fingerprint of the materials. However, despite these modifications the sorption/desorption performances remain remarkably stable for functionalized materials (surprisingly especially for MC-PYS).

3.3. Application to real effluent – acidic leachate of waste photographic film

The interest of these new sorbents for silver recovery was tested onto complex solutions (generated by the nitric acid leaching of waste photographic films). Table S16 reports the composition of the leachate (together with metal leaching efficiency; higher than 90 % for silver). After processing the sorption tests onto solutions at pH controlled close to 2.2 and 5.2, the sorption efficiencies are summarized in Table S17. The results confirm the little better efficiency of MC-PYS (compared with MC-PYO) for recovering silver from complex solution. Silver recovery (in the range 28–44 %) is systematically higher than the values reported for other metal ions. Silver sorption is better at pH_{eq} close to 2.2 compared with $\text{pH}_{\text{eq}} 5.2$.

The distribution of metals (percent, w/w) onto the sorbents depends on the sorbent and the pH (Fig. S20). However, the relative proportions follow the series: $\text{Ag(I)} > \text{Fe(III)} > \text{Al(III)} > \text{Co(II)}$. This preference is globally consistent with their relative concentrations in the leachate.

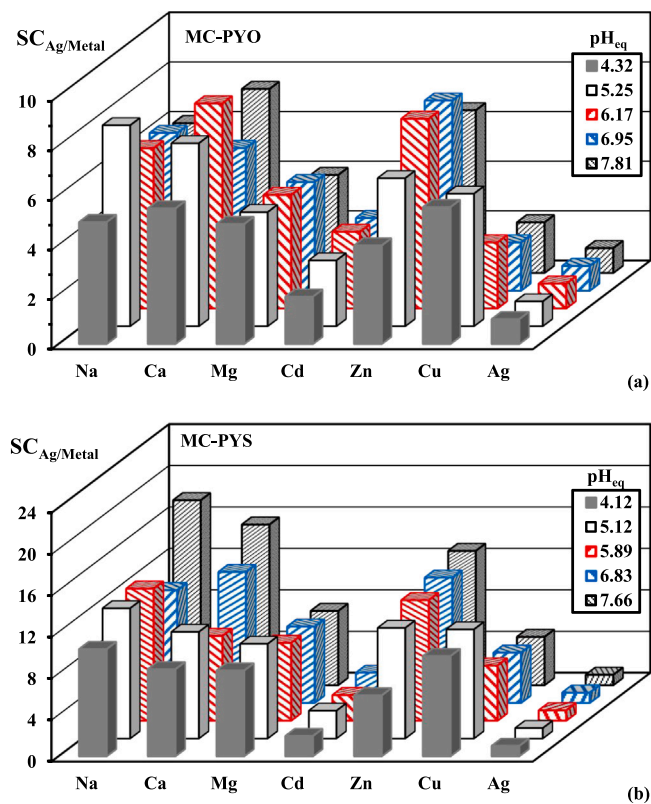


Fig. 5. Effect of pH on the selective sorption of Ag(I) using MC-PYO (a) and MC-PYS (b) (C_0 : 1 mmol L^{-1} ; T: $20 \pm 1^\circ \text{C}$, time: 24 h; v- 210 rpm, $SC_{\text{Ag}/\text{Ag}} = 1$, as reference).

Table 4

Recycling of sorbents for 5 cycles – Sorption (SE, %) and desorption (DE, %) efficiencies.

Sorbent	MC				MC-PYO				MC-PYS			
	SE (%)		DE (%)		SE (%)		DE (%)		SE (%)		DE (%)	
Cycle	Av.	StD.	Av.	StD.	Av.	StD.	Av.	StD.	Av.	StD.	Av.	StD.
1	12.5	0.2	100.5	0.6	52.0	0.5	100.1	0.4	65.8	0.9	100.3	0.6
2	12.1	0.3	100.2	1.0	51.7	0.8	100.7	1.4	65.2	0.4	100.3	0.4
3	11.7	0.6	100.1	0.0	51.5	1.1	100.5	0.1	64.8	0.3	100.0	0.2
4	11.4	0.3	100.9	0.1	51.3	1.0	100.3	0.4	64.5	0.1	100.0	0.3
5	11.2	0.4	100.1	0.1	50.8	0.6	100.1	0.1	64.2	0.3	100.0	0.2
Loss 5th/1st	10.6 %		Negligible		2.3 %		Negligible		2.4 %		Negligible	

The highest mass fraction for Ag is reported for MC-PYS when operating at pH close to 2.2: under selected experimental conditions, silver represent up to 43.6 % of total metal binding. On the opposite hand, for largest metal recovery (cumulative sorption capacity), best conditions are obtained with MC-PYS at pH 5.2, where total sorption capacity reaches 0.82 mmol g^{-1} (for $C_{\text{eq,Tot.}}: 0.103 \text{ mmol L}^{-1}$).

The selectivity coefficients $SC_{\text{Ag/Metal}}$ at $\text{pH}_{\text{eq}} \approx 2.2$ and ≈ 5.2 for both MC-PYO and MC-PYS are reported in Fig. S21. Consistently with previous conclusions, MC-PYO (hard oxygen-bearing functional groups) is less selective for silver than MC-PYS (soft sulfur-bearing functional groups). Highest selectivity for Ag(I) is reported at pH close to 5.2 with MC-PYS against:

$\text{Mg(II) (H)} > \text{Al(III) (H)} > \text{Cu(II) (B)} \approx \text{Cr(VI) (H)} \approx \text{Co(II) (B)} > \text{Ni(II) (B)} > \text{Fe(III) (H)}$.

The ranking in selectivity does not completely follow the Pearson's rules: the lowest affinity against Fe(III) breaks the trend.

It is noteworthy that the cumulative sorption capacity (appearing in Fig. S20) reaches 0.82 mmol g^{-1} for MC-PYS (0.70 mmol g^{-1} for MC-PYO), for a total initial metal concentration close to $0.514 \text{ mmol L}^{-1}$. The sorption isotherms for pure Ag(I) solutions show that for experimental conditions corresponding to the same initial Ag(I) concentration, the sorption capacity is close to $1\text{--}1.1 \text{ mmol Ag g}^{-1}$ and $0.2 \text{ mmol Ag g}^{-1}$ for MC-PYS and MC-PYO, respectively. This means that for MC-PYS, the cumulative (multi-metal) sorption capacity is of the same order of magnitude than the proper Ag sorption capacity (for the same total residual metal concentration): the reactive groups bind the other metals at the same level as silver alone. This is contrary to MC-PYO behavior: the cumulative sorption capacity is multiplied by a factor ≈ 3.5 ; meaning that the reactive groups can accommodate more easily competitor metals.

4. Conclusion

The design of magnetic chitosan particles is fundamental for simultaneously improving mass transfer properties in metal sorption and facilitating the recovering of microparticles. However, sorption performances are relatively weak and the chemical modification reveals necessary for improving the capacities of sorption. Herein, two pyrimidine-based compounds have been successfully grafted on MC and the study aimed to critically compare the sorption characteristics for Ag (I) sorption in function of the type of reactive groups (O-donor in the case of MC-PYO and S-donor for MC-PYS). Strong differences are observed in terms of sorption capacities and binding mechanisms. MC-PYO binds silver through binding onto N-based, carbonyl, hydroxyl; the sorption is exothermic. MC-PYS involves sulfur groups in endothermic metal binding. The affinity for silver is significantly higher for MC-PYS than for MC-PYO. The sulfur derivative is among the most efficient sorbents reported in literature, especially taking into account the fast kinetics. Another advantage of sulfur-derivative concerns the selectivity of MC-PYS for silver against other competitor ions (alkaline, alkaline-earth and heavy metal ions); this can be explained by the specific selectivity of sulfur groups for Ag(I) while O-bearing reactive groups have a wider reactivity for competitive cations. The application of quantitative structure-activity relationship method to the study of

sorption from multicomponent solutions confirms the predominance of covalent criterion over ionic character. This preference of MC-PYS over MC-PYO for Ag(I) is confirmed in the treatment of the leachates from waste photographic films. The functionalized sorbents (both MC-PYO and MC-PYS) have a greater stability in sorption performance at recycling, while using 0.3 M HNO_3 solutions for (total) elution of silver-loaded materials. These different properties make the sorbents very promising for silver recovery from complex solutions; however, the sulfur derivative (trithione-based sorbent) shows more attractive sorption performances both in terms of sorption capacities and selectivity.

CRedit authorship contribution statement

Mohammed F. Hamza: Conceptualization, Methodology, Software, Investigation, Resources, Writing – review & editing, Project administration, Funding acquisition. **Adel A.-H. Abdel-Rahman:** Conceptualization, Methodology, Software, Data curation. **Mohamed A. Hawata:** Formal analysis, Data curation. **Rania El Araby:** Formal analysis, Investigation, Resources. **Eric Guibal:** Conceptualization, Methodology, Software, Data curation, Writing – review & editing, Project administration, Funding acquisition. **Amr Fouda:** Formal analysis, Investigation, Resources. **Yuezhou Wei:** Conceptualization, Methodology, Software, Project administration, Funding acquisition. **Nora A. Hamad:** Formal analysis.

Declaration of Competing Interest

The authors declare that they have no known competing financial interests or personal relationships that could have appeared to influence the work reported in this paper.

Acknowledgements

W.Y acknowledges the support of National Natural Science Foundation of China [U1967218, and 11975082]. E. G., M.F.H., and A.A.-H. A-R. acknowledge the support from French Government through Institut Français d'Egypte and Egyptian Government through Academy of Science & Technology for the IMHOTEP Program (MetalValor project).

Appendix A. Supporting information

Supplementary data associated with this article can be found in the online version at [doi:10.1016/j.jece.2022.107939](https://doi.org/10.1016/j.jece.2022.107939).

References

- [1] M.D. Erku, A. Yimam, A.S. Jabasingh, Process optimization for the recovery of silver from waste X-ray photographic films, *Indian, J. Chem. Technol.* 26 (2019) 404–410.
- [2] C. Carata, E. Vasile, V.-G. Ghica, M.-I. Petrescu, G. Iacob, M. Buzatu, Recovery of silver from waste silver oxide button cells Part I: characterization of active material, *Rom. J. Mater.* 50 (2020) 191–197.
- [3] L.S. Silva de Oliveira, M.T. Weitzel Dias Carneiro Lima, L.H. Yamane, R.R. Siman, Silver recovery from end-of-life photovoltaic panels, *Detritus* 10 (2020) 62–74.

- [4] V. Savvilitidou, E. Gidarokos, Pre-concentration and recovery of silver and indium from crystalline silicon and copper indium selenide photovoltaic panels, *J. Clean. Prod.* 250 (2020), 119440.
- [5] RSC, *Periodic Table*, in: RSC (Ed.), RSC, London (UK), 2020.
- [6] H.U. Sverdrup, K.V. Ragnarsdottir, D. Koca, An assessment of metal supply sustainability as an input to policy: security of supply extraction rates, stocks-in-use, recycling, and risk of scarcity, *J. Clean. Prod.* 140 (2017) 359–372.
- [7] Z. Wang, P. Halli, P. Hannula, F. Liu, B.P. Wilson, K. Yliniemi, M. Lundstrom, Recovery of silver from dilute effluents via electrodeposition and redox replacement, *J. Electrochem. Soc.* 166 (2019) E266–E274.
- [8] N.A.D. Ho, S. Babel, Bioelectrochemical technology for recovery of silver from contaminated aqueous solution: a review, *Environ. Sci. Pollut. Res.* 28 (2020) 63480–63494.
- [9] S.-Y. Cho, T.-Y. Kim, P.-P. Sun, Recovery of silver from leachate of silicon solar cells by solvent extraction with TOPO, *Sep. Purif. Technol.* 215 (2019) 516–520.
- [10] P.-P. Sun, T.-Y. Kim, H. Seo, S.-Y. Cho, Recovery of copper(II) and silver(I) from nitrate leaching solution of industrial dust via solvent extraction with LIX63, *Metals* 11 (2021) 1300.
- [11] W.D. Xing, M.S. Lee, Development of a hydrometallurgical process for the recovery of gold and silver powders from anode slime containing copper, nickel, tin, and zinc, *Gold. Bull.* 52 (2019) 69–77.
- [12] Z. Celik, M. Guelfen, A.O. Aydin, Synthesis of a novel dithioxamide-formaldehyde resin and its application to the adsorption and separation of silver ions, *J. Hazard. Mater.* 174 (2010) 556–562.
- [13] N.B. Omar, M.L. Merroun, J.M.A. Peñalver, M.T. Gonzalez Muñoz, Comparative heavy metal biosorption study of brewery yeast and *Myxococcus xanthus* biomass, *Chemosphere* 35 (1997) 2277–2283.
- [14] M.T.K. Tsui, K.C. Cheung, N.F.Y. Tam, M.H. Wong, A comparative study on metal sorption by brown seaweed, *Chemosphere* 65 (2006) 51–57.
- [15] G.Q. Sun, X.H. Tang, L.M. Zhou, Z.R. Liu, Z.G. Le, G.L. Huang, Effective adsorption Ag(I) onto triethylenetetramine-modified chitosan beads: adsorption equilibrium, kinetic, and thermodynamic studies, *Desalin. Water Treat.* 206 (2020) 297–306.
- [16] Z. Dong, X. Yang, Q. Pan, Y. Ao, J. Du, M. Zhai, L. Zhao, Performance and mechanism of selective adsorption of silver to L-cysteine functionalized cellulose microsphere, *Cellulose* 27 (2020) 3249–3261.
- [17] M. Pilsniak-Rabiega, K. Wejman, J. Wolska, Novel conventional and chelating anion exchange resins with amino ligands for sorption of silver, *Sep. Sci. Technol.* 55 (2020) 2170–2182.
- [18] H.G. El-Shorbagy, S.M. El-Kousy, K.Z. Elwakeel, M.A. Abd El-Ghaffar, Eco-friendly chitosan condensation adduct resins for removal of toxic silver ions from aqueous medium, *J. Ind. Eng. Chem.* 100 (2021) 410–421.
- [19] C. Han, J. Li, G. Wang, C. Zhang, The adsorption of silver on powdered activated carbon in the ammonia-free thiosulfate leaching solution, *Russ. J. Non-Ferr. Met.* 62 (2021) 165–173.
- [20] G.I. Nazarchuk, I.V. Melnyk, Y.L. Zub, O.I. Makridina, A.I. Vezentsev, Mesoporous silica containing Si(CH₂)₃NHC(S)NHC₂H₅ functional groups in the surface layer, *J. Colloid Interface Sci.* 389 (2013) 115–120.
- [21] A.B. Cigil, O.A. Uruçu, H. Birtane, M.V. Kahraman, Cellulose/cysteine based thiolene UV cured adsorbent: removal of silver (I) ions from aqueous solution, *Cellulose* 28 (2021) 6439–6448.
- [22] K.Z. Elwakeel, A.S. Al-Bogami, E. Guibal, 2-Mercaptobenzimidazole derivative of chitosan for silver sorption - Contribution of magnetite incorporation and sonication effects on enhanced metal recovery, *Chem. Eng. J.* 403 (2021), 126265.
- [23] T. Onofrei, M. Albu, C. Mita, Sorption and concentration of Ag(I) on celluloses modified with azo and thiourea groups, *Cellul. Chem. Technol.* 35 (2001) 429–433.
- [24] Z. Hao, Y. Guo, P. Wu, M. Mansuer, J. Zhu, Adsorption properties of silver ions on thiourea-formaldehyde resin, 3rd International Conference on Energy, Environment and Sustainable Development (EESD 2013), Shanghai, Peoples R China, 2013, pp. 459–462.
- [25] P. Kumar, K.B. Ansari, A.C. Koli, V.G. Gaikar, Sorption behavior of thiourea grafted polymeric resin toward silver ion, reduction to silver nanoparticles, and their antibacterial properties, *Ind. Eng. Chem. Res.* 52 (2013) 6438–6445.
- [26] J.-I. Yun, S. Bhattarai, Y.-S. Yun, Y.-S. Lee, Synthesis of thiourea-immobilized polystyrene nanoparticles and their sorption behavior with respect to silver ions in aqueous phase, *J. Hazard. Mater.* 344 (2018) 398–407.
- [27] M. Pilsniak-Rabiega, J. Wolska, Silver(I) recovery on sulfur-containing polymeric sorbents from chloride solutions, *Physicochem. Probl. Miner. Process.* 56 (2020) 290–310.
- [28] P. Liu, X. Wang, L. Tian, B. He, X. Lv, X. Li, C. Wang, L. Song, Adsorption of silver ion from the aqueous solution using a polyvinylidene fluoride functional membrane bearing thiourea groups, *J. Water Process Eng.* 34 (2020), 101184.
- [29] M.A.A. El-Ghaffar, M.H. Mohamed, K.Z. Elwakeel, Adsorption of silver(I) on synthetic chelating polymer derived from 3-amino-1,2,4-triazole-5-thiol and glutaraldehyde, *Chem. Eng. J.* 151 (2009) 30–38.
- [30] I.V. Melnyk, G.I. Nazarchuk, M. Vaclavikova, Y.L. Zub, IR spectroscopy study of SBA-15 silicas functionalized with the ethylthiocarbamidepropyl groups and their interactions with Ag(I) and Hg(II) ions, *Appl. Nanosci.* 9 (2019) 683–694.
- [31] J.L. Lopes, K.L. Marques, A.V. Girao, E. Pereira, T. Trindade, Functionalized magnetite particles for adsorption of colloidal noble metal nanoparticles, *J. Colloid Interface Sci.* 475 (2016) 96–103.
- [32] R.G. Pearson, Acids and bases, *Science* 151 (1966) 172–177.
- [33] R. Massart, Preparation of aqueous magnetic liquids in alkaline and acidic media, *IEEE Trans. Magn.* 17 (1981) 1247–1249.
- [34] J.P. Gustafsson, Visual MINTEQ, (<https://vminteq.lwr.kth.se/>), Accessed: April 2019, KTH, Royal Institute of Technology, Stockholm, Sweden, 2013.
- [35] H. Prokkola, E.-T. Nurmesniemi, U. Lassi, Removal of metals by sulphide precipitation using Na₂S and HS⁻ solution, *ChemEngineering* 4 (3) (2020) 51.
- [36] C. Tien, Adsorption Calculations and Modeling, Butterworth-Heinemann, Newton, MA, 1994.
- [37] M.A. Hubbe, S. Azizian, S. Douven, Implications of apparent pseudo-second-order adsorption kinetics onto cellulosic materials: A review, *BioResources* 14 (2019) 7582–7626.
- [38] J.-P. Simonin, On the comparison of pseudo-first order and pseudo-second order rate laws in the modeling of adsorption kinetics, *Chem. Eng. J.* 300 (2016) 254–263.
- [39] Y. Marcus, Ion Properties, Marcel Dekker, Inc., N. Y., NY (1997).
- [40] H.N. Tran, E.C. Lima, R.-S. Juang, J.-C. Bollinger, H.-P. Chao, Thermodynamic parameters of liquid-phase adsorption process calculated from different equilibrium constants related to adsorption isotherms: A comparison study, *J. Environ. Chem. Eng.*, DOI <https://doi.org/10.1016/j.jece.2021.106674>(2021) 106674.
- [41] H. Shehzad, E. Ahmed, A. Sharif, M.I. Din, Z.H. Farooqi, I. Nawaz, R. Bano, M. Iftikhar, Amino-carbamate moiety grafted calcium alginate hydrogel beads for effective biosorption of Ag(I) from aqueous solution: economically-competitive recovery, *Int. J. Biol. Macromol.* 144 (2020) 362–372.
- [42] F. Wu, T. Zhao, Y. Yao, T. Jiang, B. Wang, M. Wang, Recycling supercapacitor activated carbons for adsorption of silver (I) and chromium (VI) ions from aqueous solutions, *Chemosphere* 238 (2020), 124638.
- [43] J. Wang, W. Zhang, X. Kang, C. Zhang, Rapid and efficient recovery of silver with nanoscale zerovalent iron supported on high performance activated carbon derived from straw biomass, *Environ. Pollut.* 255 (2019), 113043.
- [44] F.B. Biswas, I.M.M. Rahman, K. Nakakubo, K. Yunoshita, M. Endo, K. Nagai, A. S. Mashio, T. Taniguchi, T. Nishimura, K. Maeda, H. Hasegawa, Selective recovery of silver and palladium from acidic waste solutions using dithiocarbamate-functionalized cellulose, *Chem. Eng. J.* 407 (2021), 127225.
- [45] T. Mahlangu, R. Das, L.K. Abia, M. Onyango, S.S. Ray, A. Maity, Thiol-modified magnetic polypyrrole nanocomposite: an effective adsorbent for the adsorption of silver ions from aqueous solution and subsequent water disinfection by silver-laden nanocomposite, *Chem. Eng. J.* 360 (2019) 423–434.
- [46] C. Chen, J. Wang, Correlating metal ionic characteristics with biosorption capacity using QSAR model, *Chemosphere* 69 (2007) 1610–1616.
- [47] R. Salmimies, M. Mannila, J. Kallas, A. Häkkinen, Acidic dissolution of magnetite: experimental study on the effects of acid concentration and temperature, *Clays Clay Miner.* 59 (2011) 136–146.
- [48] M.F. Hamza, Y. Wei, A. Benettayeb, X. Wang, E. Guibal, Efficient removal of uranium, cadmium and mercury from aqueous solutions using grafted hydrazide-micro-magnetite chitosan derivative, *J. Mater. Sci.* 55 (2020) 4193–4212.